International Symposium
On Turbulence and Shear Flow
Phenomena (TSFP-9)
June 30 - July 3, 2015 *Melbourne, Australia*

CONTROL OF THE RECIRCULATION REGION OF A TRANSONIC BACKWARD-FACING STEP FLOW USING CIRCULAR LOBES

Sven Scharnowski, Istvan Bolgar, Christian J. Kähler
Institute of Fluidmechanics and Aerodynamics
Bundeswehr University Munich
85577 Neubiberg, Germany
sven.scharnowski@unibw.de

ABSTRACT

This work analyzes a backward-facing step flow and its sensitivity to disturbances at a Mach number of 0.8 and a Reynolds number of 1.8×10^5, based on the step height $h = 7.5\,\text{mm}$ and the free-stream velocity $u_\infty = 255\,\text{m/s}$. It focuses on the temporal and spatial variation of the reattachment length of a two-dimensional model with the aim to reduce and stabalize the reattachment length by means of passive flow control devises. In order to analyze the shape and dynamics of the recirculation region, the flow field in the plane of symmetry as well as in a spanwise plane slightly above the reattaching surface were measured with Particle Image Velocimetry (PIV). The mean flow reattaches ≈ 6.2 times the step height downstream of the step. It is shown that this value changes with time as much as ± 3 step heights. Horizontal measurements indicate that the strong variations of the reattachment length over the spanwise direction are associated with large–scale coherent flow structures with a dominant spanwise wave-length of ≈ 1.6 step heights. It is demonstrated the artificial generation of similar large–scale structures using circular lobes reduces the reattachment length by more than 50%. This is an important finding for flow control applications in aeronautics.

INTRODUCTION

The Backward-facing step flow has been studied extensively experimentally and numerically (Eaton & Johnston, 1981; Bradshaw & Wong, 1972). Figure 1 summarizes qualitatively the main features of the mean flow field. The incoming boundary layer developing along the forebody is forced to separate at the sharp edge of the step. As a result of Kelvin-Helmholtz instabilities, tiny spanwise vortices are generated in the first part of the very thin shear layer. The vortices grow in size while convecting downstream. According to Simpson (1989), the spanwise coherence starts to break down after 3 step heights due to secondary instabilities and strong non-linear interactions. This on average causes an increased broadening of the shear layer with increasing distance from the point of separation. Due to the enhanced turbulent mixing, high momentum zones are transported towards the wall, causing the shear layer to reattach on the splitter plate. The mean flow field is characterized by a large recirculation region and an outer flow region separated up by a dividing streamline. The reattachment location is not fixed in space and time due to the dynamics of turbulent structures.

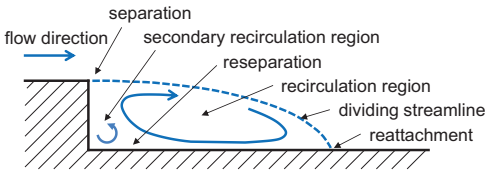

Figure 1: Backward–facing step mean flow field.

Bradshaw & Wong (1972) as well as Eaton & Johnston (1981) showed in their review papers, that for two–dimensional flows around a backward–facing step, the streamwise extension of the primary recirculation region mainly depends on the step height h and the state of the incoming boundary layer. The reattachment length is between $5h$ to $7h$ for a fully turbulent incoming flow state at the point of separation. This holds for a Reynolds number range of $\text{Re}_\text{h} = 3000 - 300\,000$. Simpson (1989) showed in his review paper, that the instantaneous impingement location of the shear layer moves up- and downstream by as much as $\pm 2h$. According to Driver *et al.* (1987), the non-dimensional frequency of this motion is $f \cdot x_r / u_\infty \approx 0.6 - 0.8$. In this paper two questions will be addressed: (1) Are the fluctuations of the reattachment line caused by large-scale coherent flow structures? (2) If so, can the reattachment line be stabilized and its distance from the step reduced by generating artificial large–scale flow structures using circular lobes?

Therefore, planar PIV measurements of a two–dimensional backward-facing step at a free stream Mach number of 0.8 and a Reynolds number of 1.8×10^5, based on the step height $h = 7.5\,\text{mm}$ and the free-stream velocity $u_\infty = 255\,\text{m/s}$ were performed. The transonic Mach number was chosen because of its importance for aeronautical applications in this regime.

MEASUREMENT SETUP

The measurements were performed in the Trisonic Wind tunnel at the Bundeswehr University in Munich (TWM). The TWM facility is a blow-down type wind tunnel with a 300 mm $\times$ 675 mm (w $\times$ h) test section, with a stable operating range of Mach numbers from 0.2 to 3.0. It has two tanks that can be pressurized up to 20 bar above ambient pressure, holding a total volume of 356 m^3 of dry

air. To control the Reynolds number, the total pressure in the test section is varied between 1.2 to 5 bar. The facility is discussed in detail in Bitter *et al.* (2011). The total pressure and the total temperature for the discussed measurements were $p_0 = 1.73\,\text{bar}$ and $T_0 = 285\,\text{K}$, respectively.

For the PIV experiments a quasi-2D model is being utilized, as sketched in Figure 2. The model spans across the entire test section (300 mm) and is symmetric about its horizontal plane. It features a 150 mm long nose followed by 100 mm long main body and a 125 mm long splitter plate. The nose's design and its smooth connection to the main body ensure a shock free flow around the model at Mach 0.8. The thickness of the model's main part is 25 mm and the step height between main body and splitter plate is 7.5 mm. Thus, the area aspect ratio for the sudden step is 1:1.02. A ratio of 1:40 was achieved for step height to step width, which ensures that the wind tunnel side walls did not affect the recirculation region (Eaton & Johnston, 1981).

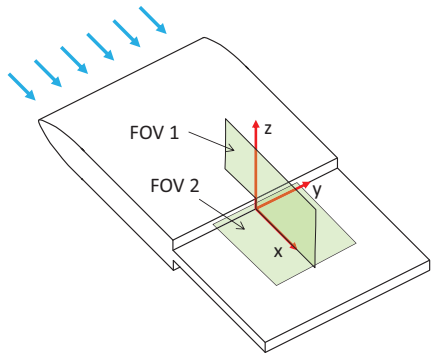

Figure 2: Sketch of the model and the fields of view (FOV).

The flow was seeded with Di-Ethyl-Hexyl-Sebacat (DEHS) tracer particles with a mean diameter of 1 μm, as described by Kähler *et al.* (2002). Planar measurements were performed in two fields of view (FOV): in the vertical plane of symmetry and in a spanwise plane just above the reattaching surface. The particles in the desired plane were illuminated by a laser light sheet. In order to analyze the wake flow in detail, 4000 and 2000 PIV double images, 2560×2160 pixel in size, were recorded at statistically independent time steps for the vertical and horizontal planes, respectively. The time between the double images was set to $2\,\mu$s, corresponding to 15 pixel particle images shift at free stream velocity, in order to avoid bias errors due to curved streamlines (Scharnowski & Kähler, 2013). For the data evaluation iterative window correlation including image deformation and Gaussian window weighting was applied. The final interrogation-window size was set to 16×16 pixel with an overlap of 50%, leading to a vector grid spacing of $250\,\mu$m (or 3.3% of the step height). In a post-processing step vectors that differ by more than two times the standard deviation of their neighbors from the median of the neighbors (for each component) were replaced with the median value of the neighbors in order to reject outliers.

RESULTS AND DISCUSSION

Vertical plane

The evaluation of the vertical plane of symmetry revealed the known strong fluctuations in the recirculation region. Figure 3 illustrates two snap shots showing extreme cases with weak (top) and very strong (middle) back flow. In the case of weak back flow the wake is characterized by a large region with low momentum. Several spots with reversed flow can be found close to the splitter plate between $x/h = 2$ and 6. The back flow velocity reaches values up to $u/u_\infty \approx -0.2$. In contrast, for the case of strong back flow, the wake region features a large region with reversed flow between $x/h = 2$ and 6 in which the back flow velocities reach values up to $u/u_\infty < -0.5$. Among the 4000 measured velocity fields, the back flow regions' size and the maximum upstream velocity lies in between the two cases from Figure 3 for most instantaneous distributions. Figure 3 on the bottom shows the mean flow field computed with single-pixel evaluation to achieve improved resolution (Kähler *et al.*, 2006, 2012). The averaged flow field is characterized by a large recirculation region with a maximum upstream mean velocity of $u/u_\infty \approx -0.2$. In the corner of the step a secondary recirculation region with opposite rotation direction was resolved. The mean velocity distribution is similar to those of low Reynolds number flows over backward-facing steps.

In order to analyze the dynamics of the recirculation region statistically, the back flow ratio with respect to the streamwise location computed from all 4000 instantaneous flow fields is shown in Figure 4 for different heights over the splitter plate. The figure shows that the strongest back flow is at a height of $z/h \approx 0.1$, reaching 96% at $x/h \approx 2.7$. In the secondary recirculation region the back flow ratio reaches a minimum of $\approx 22\%$ at $x/h \approx 0.3$, and rises again further upstream. The back flow distributions at $z/h = 0.3$ and 0.5 are characterized by a lower maximum that is shifted upstream.

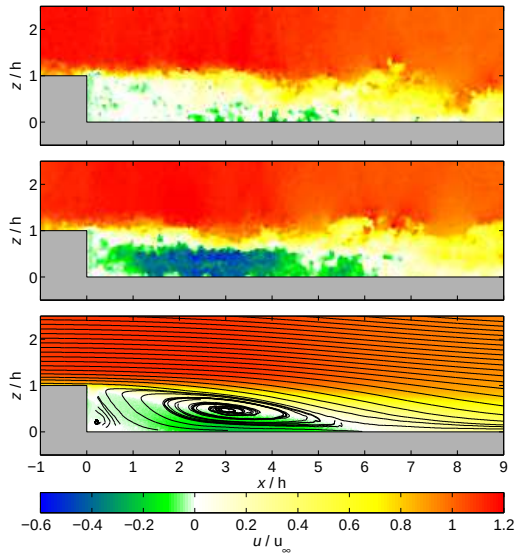

Figure 3: Two extreme cases of the instantaneous streamwise velocity distribution with weak (top) and strong (middle) back flow and the mean velocity distribution (bottom).

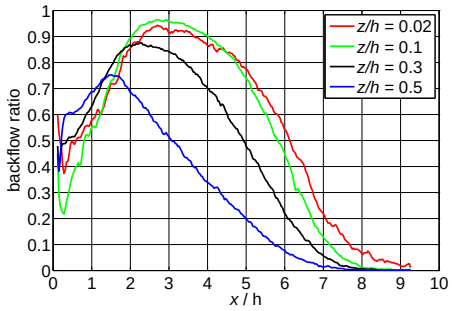

Figure 4: Back flow ratio in the recirculation region for different heights over the splitter plate.

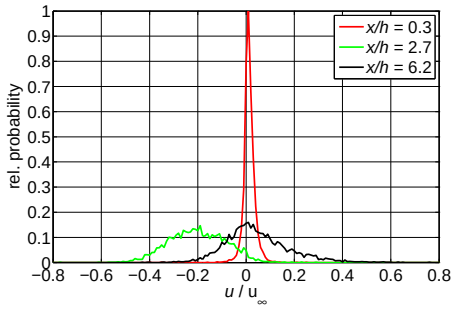

Figure 5: Histogram of the streamwise velocity at a wall distance of $z/h = 0.1$ for three streamwise locations: minimum back flow, maximum back flow, and mean reattachment.

The presented near-wall back flow differs from the results presented by Tihon *et al.* (2001) for Reynolds numbers up to $\mathrm{Re_h} = 4800$. For their experiments the back flow ratio is $< 3\%$ in the secondary recirculation region with a minimum of 0% and reaches 100% in the center of the primary recirculation region. From this differences it can be concluded that the low Reynolds number case (Tihon *et al.*, 2001) features a rather stable combination of primary and secondary recirculation region while the high Reynolds number case (present) does not. Meaning that in any location inside the recirculation region the fluid motion can be upstream or downstream since the back flow ratio does not reach 0% or 100%, according to Figure 4.

The mean reattachment location is an important parameter of backward-facing step flow. From the most near-wall graph at $z/h = 0.02$ the mean reattachment location is deduced from the back flow ratio of 0.5 to be $x_r/h \approx 6.2$. The mean reattachment location is within the range of other 2D experiments (Bradshaw & Wong (1972); Eaton & Johnston (1981)) and it is shifted downstream compared to the axisymmetric case (Scharnowski & Kähler (2015); Deck & Thorigny (2007)). It is important to note that for this graph the probability of having back flow does not drop to zero until $x/h = 9$, which was the end of the measurement area. Thus, regions with recirculating fluid can be found as far downstream as $x/h = 9$. For the location of maximum back flow ratio, $x/h = 2.7$, the probability distribution of the streamwise velocity in Figure 5 shows a broad peak. The velocity varies between $u/u_\infty = -0.55 \leq$ and $u/u\infty = +0.15$ and has its maximum at $u/u_\infty \approx -0.2$. Thus, for some snap shots the streamwise velocity is positive at $x/h = 2.7$ while for others it is negative at $x/h = 9$. Such strong variations of the recirculation region have not been reported for experiments at low Mach numbers or in incompressible flow (Simpson, 1989; Adams & Johnston, 1988). In the secondary recirculation region at $x/h = 0.3$ the streamwise velocity varies between $u/u_\infty = -0.12 \leq$ and $u/u_\infty = +0.14$, according to Figure 5. At the mean reattachment location $x/h = 6.2$ the highest probability is at $u = 0\,\mathrm{m/s}$. However, the probability distribution has roughly the same width as for the $x/h = 2.7$. The shape of the distribution at mean reattachment is slightly skewed towards positive velocities.

Horizontal plane

To examine if the large variations of the reattachment location is associated with large–scale coherent flow structures measurements were performed in a horizontal plane. The PIV investigation of the flow field on the vertical plane of symmetry (FOV 1 in Figure 2) shows that the variation of the reattachment line is associated with large–scale flow structures. In order to analyze the spanwise extension of the flow features from Figure 3, a horizontal plane above the splitter plate at $z/h \approx 0.25$ was investigated. Figure 6 illustrates a characteristic snap shot of the horizontal velocity component for FOV 2 (compare Figure 2). In the vicinity of the reattachment location a coherent pattern of elongated finger–like turbulent flow structures is visible. The variation of the recirculation region from Figure 3 can now also be deduced from a single instantaneous horizontal velocity field. Thus, the variation of the recirculation region's size is caused by large–scale spatial fluctuations, which change over time and which seem to have a certain span-wise extend and periodicity.

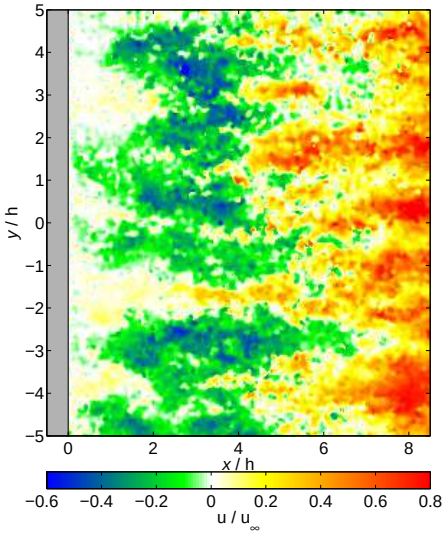

Figure 6: Instantaneous distribution of the streamwise velocity component in the vicinity of the splitter plate's surface ($z/h \approx 0.25$).

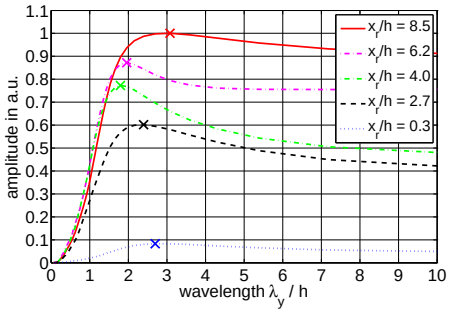

Figure 7: Power spectral density of the the streamwise velocity fluctuations in the vicinity of the splitter plate's surface ($z/h \approx 0.25$) along the spanwise direction for different streamwise locations with respect to the wave length (inverse spatial frequency).

The size distribution was estimated by computing the power spectral density of the velocity fluctuations along the spanwise direction using the method of Welch (1967). The size of the structures is then given by the wave length of the corresponding spatial frequencies. The spectral amplitude over the wavelength λ is illustrated in Figure 7 for 5 different streamwise locations, ranging from $x/h = 0.3$ to $x/h = 8.5$. The graphs are averaged over 2000 velocity fields. At the mean reattachment location as well as further upstream ($x/h = 2.7 - 6.2$) the distribution features a distinct maximum at around $\lambda_y/h = 2$, corresponding to a structure size of $\lambda_y \approx 2 \cdot h$. Furthermore, it can be seen that the maximum of the different graphs in Figure 7 shifts towards slightly larger structures for locations before ($x_r/h = 0.3$ and 2.7) and after ($x_r/h = 8.5$) the mean reattachment compared to the peak close to reattachment ($x_r/h = 6.2$). At $x_r/h = 8.5$ these small structures are less dominant. From the figure it is evident that large–scale coherent flow structures exist in the analyzed flow and dominate its dynamics.

To investigate the shape and size of the coherent flow structures in more detail, the two point correlation function was calculated from the instantaneous velocity fields. For the velocity component u, the two-point correlation coefficient is defined as

$$R_{\mathrm{uu}}(x_0, y_0, x, y) = \frac{\sum_{n=1}^{N} u'_{\mathrm{n}}(x_0, y_0) \cdot u'_{\mathrm{n}}(x, y)}{\sigma_{\mathrm{u}}(x_0, y_0)\, \sigma_{\mathrm{u}}(x, y)} \qquad (1)$$

where N is the total number of vector fields, n is the corresponding control variable, $u'_{\mathrm{n}} = u_{\mathrm{n}} - \langle u \rangle$ is the velocity fluctuation component, and σ_{u} is the velocitys standard deviation. An ensemble of PIV vector fields allows for the correlation of the point of interest (x_0, y_0) with all points within the field of view (x, y).

Figure 8 shows the spatial distribution of the two-point correlation coefficient R_{uu} of the streamwise velocity. Since the R_{uu} distribution is rather independent from the spanwise location for the investigated geometry, the results in Figure 8 were averaged over $-1.5 \leq y/h \leq 1.5$ to enhance the contrast. It can be seen from the figure that large coherent structures develop in the separated region in accordance with Figure 6. The region of positive correlation is stretched in the streamwise direction similar to the finger–like structures

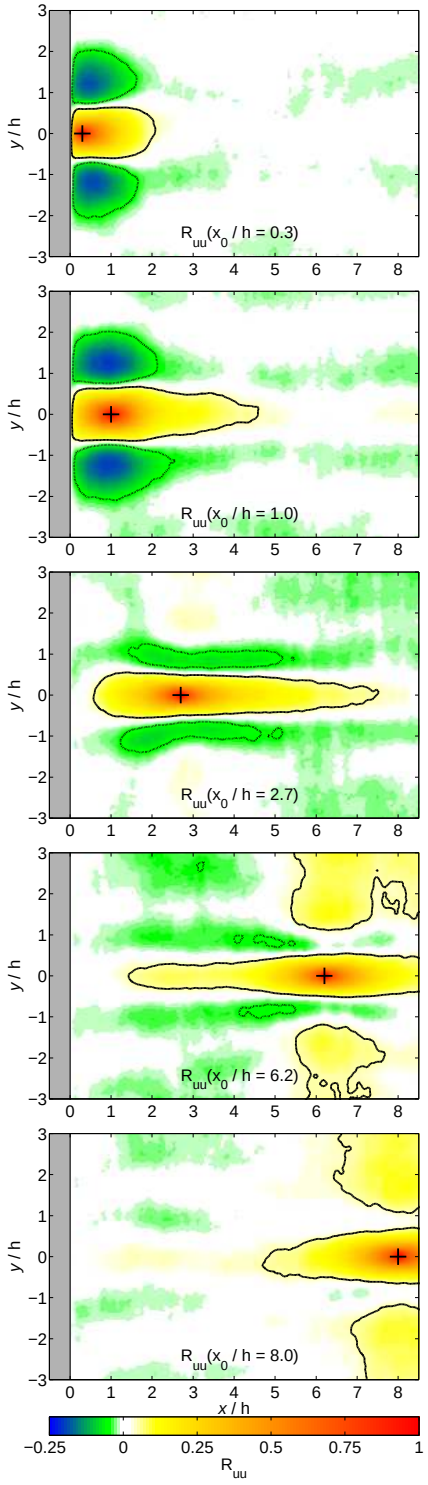

Figure 8: Two point correlation of the streamwise velocity for different streamwise locations. Contour lines are indicating the $\pm 5\%$ level.

from Figure 6. Furthermore, inside the recirculation region ($x/h \leq 6.2$) the positive correlation of R_{uu} is accompanied by regions of negative correlation. Thus, coherent structures with different velocities are well organized in span-wise direction. The streamwise extension of the regions with posi-

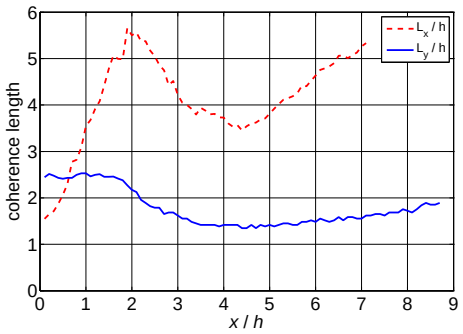

Figure 9: Streamwise coherence length L_x and distance between minima L_y extracted from R_{uu}.

tive correlation L_x is plotted in Figure 9 with respect to the streamwise location, where L_x is the streamwise distance from the correlation maximum to the location with 5% correlation value. Structures with $L_x/h > 5$ exist in the first part of the shear layer as well as close to reattachment. Figure 9 also shows the distance between the minima in the two negative correlation regions. This distance is largest within the secondary recirculation region where the negative correlation also is strongest. The estimated structure size from the power spectral density in Figure 7 matches well with the two point correlation results. Downstream of reattachment (at $x/h = 8$) larger spanwise structures with weak correlation are detected.

Reduced recirculation region

To study the sensitivity of the reattachment length with respect to coherent flow structures, artificial structures were generated using vortex generators with different amplitude and wavelength. Isomoto & Honami (1989) showed that the reattachment length can be controlled by means of spanwise vortex generators: They were able to reduce the reattachment length by up to 25% by increasing the turbulence in the incoming boundary layer via spanwise cavities or rods.

As the wake flow is dominated by finger–like large–scale coherent flow structures according to the previous section, it was the aim of the study to examine the effect of artificial finger–like structures, which are even more coherent than the natural ones, on the reattachment length and dynamics. Therefore, circular lobes of different shapes have been used (Waitz *et al.*, 1997). The Lobes consist of alternating valleys and peaks with a slope of $\pm 18^\circ$ with respect to the x–axis, see Figure 10. The periodicity was set to $1.6h$ in order match the spanwise structure size L_y. Since the shape of the lobes is circular the step's edge is modulated with an amplitude of $\pm 0.4h$. With this approach the wake flow is highly ordered until $x/h \approx 3$ in spanwise direction, as shown in Figure 11. In the valleys of the lobes the flow is accelerated while behind the peaks recirculation occurs. Upstream and downstream flowing regions exist side by side and their pattern is now fixed due to the lobes at the step. This results in coherent structures with a preferred size, as illustrated in the spectrum in Figure 12. The lobes generate streamwise aligned vortices which enhance the momentum transfer between the finger–like structures of the wake and in wall-normal direction. In effect the shear layer is subject to strong mixing and broadens rapidly. As a result it reattaches much earlier than for the clean case. This can be seen in Figure 13 which shows the streamwise mean velocity distribution in a vertical plane at a lobe's peak. The streamlines in the figure indicate a strong three–dimensional mean flow topology: The plane at the lobe's peak shows a fluid source in the vicinity of the splitter plate around $x/h = 1.5$ and a fluid drain close to the step at $x/h \approx 0.2$ and $y/h \approx 0.8$. On the one hand, the fluid flowing through the valleys reattaches very early at $x/h \approx 1.0$ (not shown in the figure) and is than transported in spanwise direction towards the wake of the peaks. On the other hand, the fluid behind the peaks is pushed outwards in the drain indicated by the inwards bending streamlines close to the step. In the mean flow field the reattachment occurs between $x/h = 1$ and $x/h = 2$ depending on the spanmwise location and the recirculation region extends to $x/h \approx 2.5$ behind the lobe's peaks. In comparison with the clean case of the backward-facing step (Figure 3) an enormous reduction of the recirculation region was achieved by stabilizing

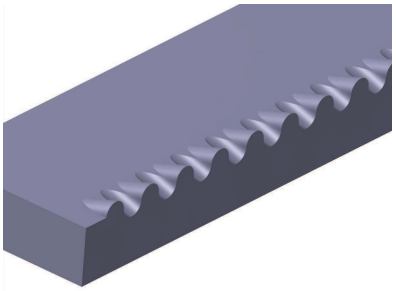

Figure 10: Sketch of the wavy trailing edge: So-called circular lobes are used to enhance shear layer mixing.

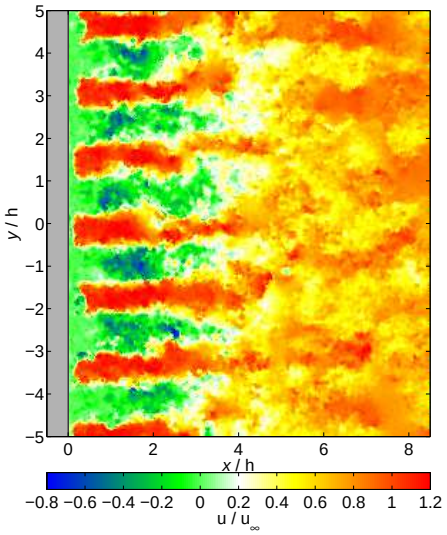

Figure 11: Instantaneous distribution of the streamwise velocity component at $z/h \approx 0.7$ in the wake of a backward-facing step with passive flow control via circular lobes which match the periodicity of natural coherent structures.

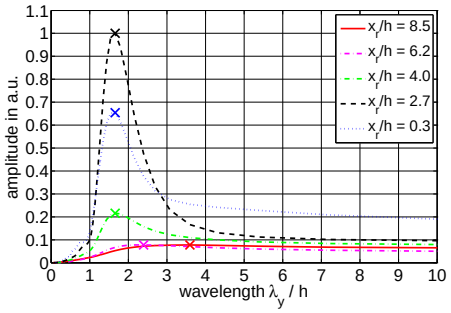

Figure 12: Power spectral density of the the streamwise velocity fluctuations at $z/h \approx 0.7$ along the spanwise direction for different streamwise locations with respect to the wave length (inverse spatial frequency) for the wavy edge of the step.

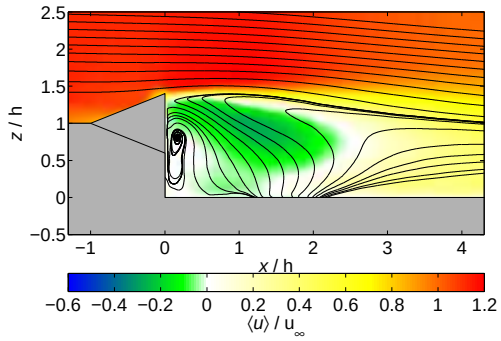

Figure 13: Backward-facing step flow with reduced recirculation region due to a wavy trailing edge of the step.

and mixing the natural structures with passive flow control.

CONCLUSIONS

It was shown that the finger–like large–scale coherent flow structures exist in the turbulent wake behind a backward-facing step. The structures have a prefered periodicity in the spanwise direction of $\lambda_y \approx 1.6h$ and an average length of arround $5h$. The strong variation of the reattachment position observed in many previous investigations, is a direct consequence of these coherent structures and their spatial random organization. It could be shown that the generation of similar structures, which are spatially fixed, allows to reduce the dynamics of the reattachment location strongly. Furthermore, the streamwise extension of the reattachment region is reduced by more than 50% if the spatial frequency and amplitude of the finger–like coherent flow structures are well selected. These findings open the door for efficient flow control in aeronautics, where backward-facing steps are omnipresent.

ACKNOWLEDGMENTS

Financial support from the German Research Foundation in the framework of the TRR 40 –Technological foundations for the design of thermally and mechanically highly loaded components of future space transportation systems– is gratefully acknowledged by the authors.

REFERENCES

Adams, E. W. & Johnston, J. P. 1988 Flow structure in the near-wall zone of a turbulent separated flow. *AIAA journal* **26** (8), 932–939.

Bitter, M., Scharnowski, S., Hain, R. & Kähler, C. J. 2011 High-repetition-rate PIV investigations on a generic rocket model in sub- and supersonic flows. *Exp Fluids* **50**, 1019–1030.

Bradshaw, P. & Wong, F. Y. F. 1972 The reattachment and relaxation of a turbulent shear layer. *J Fluid Mech* **52**, 113–135.

Deck, S. & Thorigny, P. 2007 Unsteadiness of an axisymmetric separating-reattaching flow: Numerical investigation. *Phys Fluids* **19**, 065103.

Driver, D. M., Seegmiller, H. L. & Marvin, J. G. 1987 Time-dependent behavior of a reattaching shear layer. *AIAA journal* **25** (7), 914–919.

Eaton, J. K. & Johnston, J. P. 1981 A Review of Research on Subsonic Turbulent Flow Reattachment. *AIAA Journal* **19**, 1093–1100.

Isomoto, K. & Honami, S. 1989 The Effect of Inlet Turbulence Intensity on the Reattachment Process over Backward-Facing Step. *Journal of Fluids Engineering* **111**, 87–92.

Kähler, C. J., Sammler, B. & Kompenhans, J. 2002 Generation and control of particle size distributions for optical velocity measurement techniques in fluid mechanics. *Exp Fluids* **33**, 736–742.

Kähler, C. J., Scharnowski, S. & Cierpka, C. 2012 On the resolution limit of digital particle image velocimetry. *Exp Fluids* **52**, 1629–1639.

Kähler, C. J., Scholz, U. & Ortmanns, J. 2006 Wall-shear-stress and near-wall turbulence measurements up to single pixel resolution by means of long-distance micro-PIV. *Exp Fluids* **41**, 327–341.

Scharnowski, S. & Kähler, C. J. 2013 On the effect of curved streamlines on the accuracy of PIV vector fields. *Experiments in Fluids* **54**, 1435.

Scharnowski, S. & Kähler, C. J. 2015 Investigation of a transonic separating/reattaching shear layer by means of PIV. *Theoretical and Applied Mechanics Letters* **5**, 30–34.

Simpson, R. L. 1989 Turbulent boundary-layer separation. *Annual Review of Fluid Mechanics* **21**, 205–232.

Tihon, J., Legrand, J. & Legentilhomme, P. 2001 Near-wall investigation of backward-facing step flows. *Experiments in Fluids* **31** (5), 484–493.

Waitz, I. A., Qiu, Y. J., Manning, T. A., Fung, A. K. S., Elliot, J. K., Kerwin, J. M., Krasnodebski, J. K., O'Sullivan, M. N., Tew, D. E., Greitzer, E. M., Marble, F. E., Tan, C. S. & Tillman, T. G. 1997 Enhanced mixing with streamwise vorticity. *Progress in Aerospace Sciences* **33** (5), 323–351.

Welch, P. D. 1967 The Use of Fast Fourier Transform for the Estimation of Power Spectra: A Method Based on Time Averaging Over Short, Modified Periodograms. *IEEE Trans. Audio Electroacoustics* **AU-15**, 70–73.